

Lawin Transformer: Improving Semantic Segmentation Transformer with Multi-Scale Representations via Large Window Attention

Haotian Yan, Chuang Zhang and Ming Wu
 Pattern Recognition and Intelligent System Lab,
 Beijing University of Posts and Telecommunications
 {yanhaotian, zhangchuang, wuming}@bupt.edu.cn

Abstract

*Multi-scale representations are crucial for semantic segmentation. The community has witnessed the flourish of semantic segmentation convolutional neural networks (CNN) exploiting multi-scale contextual information. Motivated by that the vision transformer (ViT) is powerful in image classification, some semantic segmentation ViTs are recently proposed, most of them attaining impressive results but at a cost of computational economy. In this paper, we succeed in introducing multi-scale representations into semantic segmentation ViT via window attention mechanism and further improves the performance and efficiency. To this end, we introduce large window attention which allows the local window to query a larger area of context window at only a little computation overhead. By regulating the ratio of the context area to the query area, we enable the large window attention to capture the contextual information at multiple scales. Moreover, the framework of spatial pyramid pooling is adopted to collaborate with the large window attention, which presents a novel decoder named **large window attention spatial pyramid pooling (LawinASPP)** for semantic segmentation ViT. Our resulting ViT, **Lawin Transformer**, is composed of an efficient hierarchical vision transformer (HVT) as encoder and a LawinASPP as decoder. The empirical results demonstrate that Lawin Transformer offers an improved efficiency compared to the existing method. Lawin Transformer further sets new state-of-the-art performance on Cityscapes (84.4% mIoU), ADE20K (56.2% mIoU) and COCO-Stuff datasets. The code will be released at <https://github.com/yan-hao-tian/lawin>.*

1. Introduction

Semantic segmentation is one of the most significant dense prediction tasks in computer vision. With the prosperity of deep convolutional neural network (CNN) in this field, the CNN-based semantic segmentation pipeline gains

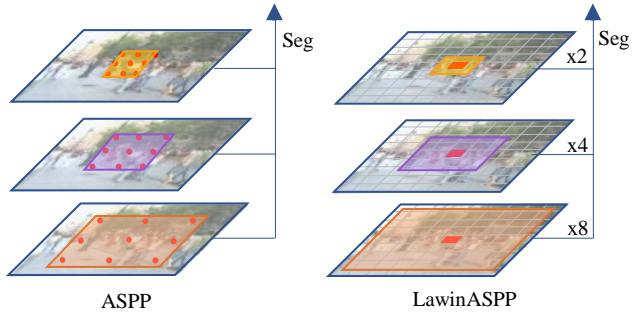


Figure 1. Difference between LawinASPP and ASPP. In ASPP, atrous convolution with different dilation rates captures representations at multiple scales. In contrast, LawinASPP replaces atrous convolution with our proposed *large window attention*. The red window represents the query area. The yellow, orange and purple windows represent the context area with different spatial sizes.

more and more popularity in a wide range of practical applications such as self-driving cars, medical imaging analysis and remote sensing imagery interpretation [32, 34, 35]. Having scrutinized the famed semantic segmentation CNN, we note that a series of work largely focus on exploiting multi-scale representations [9, 10, 24, 25, 49, 50], which plays a vital role of understanding the context prior at multiple scales. To incorporate the rich contextual information, most of these works apply filters or pooling operations, such as atrous convolution [47] and adaptive pooling, to the spatial pyramid pooling (SPP) module [23, 27].

Since the impressive performance of Vision Transformer (ViT) on image classification [19, 38], there are some efforts to resolve semantic segmentation with pure transformer models, still outperforming the previous semantic segmentation CNN by a large margin [30, 36, 42, 52]. However, it takes a very high computation cost to implement these semantic segmentation ViTs, especially when the input image is large. In order to tackle this issue, the method purely based on the hierarchical vision transformer (HVT)

has emerged with saving much computational budget. Swin Transformer is one of the most representative HVTs achieving state-of-the-art results on many vision tasks [30], whilst it employs a heavy decoder [42] to classify pixels. SegFormer refines the design of both encoder and decoder, resulting a very efficient semantic segmentation ViT [43]. But it is problematic that SegFormer solely relies on increasing the model capacity of encoder to progressively improve performance, which has a potentially lower efficiency ceiling.

Through the above analysis, we think one major problem for current semantic segmentation ViT is lack of multi-scale contextual information, thus impairing the performance and efficiency. To overcome the limitation, we present a novel window attention mechanism named *large window attention*. In large window attention, the uniformly split patch queries the context patch covering a much larger region as illustrated in Fig 1, whereas the patch in *local window attention* merely queries itself. On the other hand, considering that the attention would become computationally prohibitive with the enlargement of context patch, we devise a simple yet effective strategy to alleviate the *dilemma of large context*. Specifically, we first pool the large context patch to spatial dimension of the corresponding query patch in order to preserve the original computational complexity. Then we enable the multi-head mechanism in large window attention and set the number of head strictly equal to the square of the downsampling ratio R while pooling the context, mainly for recovering the discarded dependencies between query and context. Finally, inspired by token-mixing MLP in MLP-Mixer [37], we apply R^2 *position-mixing* operations on the R^2 subspaces of head respectively, strengthening the spatially representational power of multi-head attention. Therefore, the patch in our proposed large window attention can capture contextual information at any scales, merely yielding a little computational overhead caused by *position-mixing* operations. Coupled with large window attention with different ratios R , a SPP module evolves into a *large window attention spatial pyramid pooling* (LawinASPP), which one can employ like ASPP (Atrous Spatial Pyramid Pooling) [9] and PPM (Pyramid Pooling Module) [50] to exploit multi-scale representations for semantic segmentation.

We extend the efficient HVT to Lawin Transformer by placing the LawinASPP at the top of HVT, which introduces the multi-scale representations into the semantic segmentation ViT. The performance and efficiency of Lawin Transformer is evaluated on Cityscapes [17], ADE20K [53] and COCO-Stuff [4] datasets. We conduct extensive experiments to compare Lawin Transformer with existing HVT-based semantic segmentation method [11, 30, 43]. An improved efficiency of Lawin Transformer is proved by that Lawin Transformer spends less computational resource in attaining the better performance. Besides, our experiments

show that Lawin Transformer outperforms other state-of-the-art methods consistently on these benchmarks.

2. Related Work

2.1. Semantic Segmentation

Semantic segmentation models based on fully convolutional neural network (FCN) [31] are the most promising ways to accomplish the pixel-level classification. Towards precise scene understanding, consecutive improvements have been developed for semantic segmentation CNN in many aspects. [1, 3, 29, 34] mitigates the boundary information shortage of high-level feature. [7, 8, 33, 47] are proposed to enlarge the receptive field of model. The spatial pyramid pooling (SPP) module has proved to be effective in exploiting multi-scale representations, which gathers scene clues from local context to global context [10, 24, 25, 50]. An alternative line of work utilizes the variants of self-attention mechanism to model dependencies among representations [5, 21, 26, 28, 40, 45, 46, 51].

2.2. Vision Transformer

Transformer has revolutionized neural language processing and proven extremely successful in computer vision. ViT [19] is the first end-to-end Vision Transformer for image classification by projecting the input image into a token sequence and attach it to a class token. DeiT [38] improves the data efficiency of training ViT with a token distillation pipeline. Apart from the sequence-to-sequence structure, the efficiency of PVT [39] and Swin Transformer [30] sparks much interests in exploring the Hierarchical Vision Transformer (HVT) [14, 22, 41, 44]. ViT is also extended to solve the low-level tasks and dense prediction problems [2, 6, 20]. Specially, concurrent semantic segmentation methods driven by ViT presents impressive performance. SETR [52] deploys the ViT as an encoder and upsamples the output patch embedding to classify pixels. Swin Transformer extends itself to a semantic segmentation ViT by connecting a UpNet [42]. Segmener [36] depends on the ViT/DeiT as backbone and propose a mask Transformer decoder. Segformer [43] shows a simple, efficient yet powerful design of encoder and decoder for semantic segmentation. MaskFormer [11] reformulates the semantic segmentation as a mask classification problem, having much fewer FLOPs and parameters compared to Swin-UpNet. In this paper, we take a new step towards a more efficient design of semantic segmentation ViT, by introducing multi-scale representations into the HVT.

2.3. MLP-Mixer

MLP-Mixer [37] is a novel neural network much simpler than ViT. Similar to ViT, MLP-Mixer first adopts a linear projection to obtain a token sequence like ViT. The

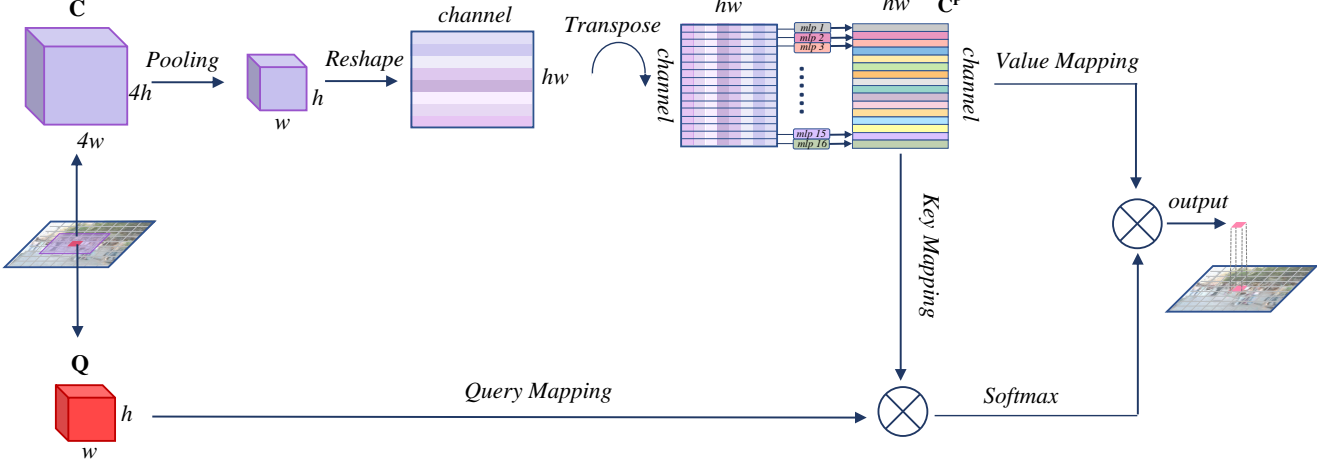


Figure 2. A large window attention. The red patch \mathbf{Q} is the query patch and the purple patch \mathbf{C} is the context patch. The context is reshaped and fed into token-mixing MLPs. The output context \mathbf{C}^P is named *position-mixed context*. Best viewed in color.

sharp distinction is that MLP-Mixer is entirely based on multi-layer perceptrons (MLP), because it replaces the self-attention in transformer layer with the token-mixing MLP. Token-Mixing MLP acts along the channel dimension, mixing the token (position) to learn spatial representations. In our proposed large window attention, token-mixing MLP is applied to the pooled context patch, which we call *position-mixing* to boost the spatial representations of multi-head attention.

3. Method

In this part, we first briefly introduce multi-head attention and token-mixing MLP. Then we elaborate large window attention and describe the architecture of LawinASPP. Finally, the overall structure of Lawin Transformer is presented.

3.1. Background

Multi-head attention is the core of Transformer layer. In the Hierarchical Vision Transformer (HVT), the operation of multi-head attention is limited to local uniformly split window, which is called local window attention. Assuming the input is a 2D feature map denoted as $\mathbf{x}_{2d} \in \mathbb{R}^{C \times H \times W}$, we can formulate the action of window attention as:

$$\hat{\mathbf{x}}_{2d} = \text{Reshape} \left(h, \frac{HW}{P^2}, \frac{C}{h}, P, P \right) (\mathbf{x}_{2d}), \quad (1)$$

$$\mathbf{x}_{2d} = \text{Reshape} (C, H, W) (\text{MHA} (\hat{\mathbf{x}}_{2d})) + \mathbf{x}_{2d}, \quad (2)$$

where h is the head number and P is the spatial size of windows, and $\text{MHA} (\cdot)$ is the Multi-Head Attention (MHA) mechanism. The basic operation of MHA can be described

as:

$$A = \text{softmax} \left(\frac{(\mathbf{W}_q \mathbf{x}_{2d})(\mathbf{W}_k \mathbf{x}_{2d})^T}{\sqrt{D_h}} \right) (\mathbf{W}_v \mathbf{x}_{2d}), \quad (3)$$

$$\text{MHA} = \text{concat} [A_1; A_2; \dots; A_h] \mathbf{W}_{\text{mhsa}}, \quad (4)$$

where \mathbf{W}_q , \mathbf{W}_k and $\mathbf{W}_v \in \mathbb{R}^{C \times D_h}$ are the learned linear transformations and $\mathbf{W}_{\text{mhsa}} \in \mathbb{R}^{D \times C}$ is the learned weights that aggregates multiple attention values. D_h is typically set to D/h and D is the embedding dimension.

Token-mixing MLP is the core of MLP-Mixer which can aggregate spatial information, by allowing the spatial position to communicate each other. Given the input 2D feature map $\mathbf{x}_{2d} \in \mathbb{R}^{C \times H \times W}$, the operation of token-mixing MLP can be formulated as:

$$\hat{\mathbf{x}}_{2d} = \text{Reshape} (C, HW) (\mathbf{x}_{2d}), \quad (5)$$

$$\mathbf{x}_{2d} = \text{Reshape} (C, H, W) (\text{MLP} (\hat{\mathbf{x}}_{2d})) + \mathbf{x}_{2d}, \quad (6)$$

$$\text{MLP} (\mathbf{x}_{2d}) = \mathbf{W}_2 \sigma (\mathbf{W}_1 \mathbf{x}_{2d}), \quad (7)$$

where $\mathbf{W}_1 \in \mathbb{R}^{HW \times D_{\text{mlp}}}$ and $\mathbf{W}_2 \in \mathbb{R}^{D_{\text{mlp}} \times HW}$ are both learned linear transformations, and σ is the activation function providing non-linearity.

3.2. Large Window Attention

Similar with window attention mentioned in section 3.1, large window attention splits the entire feature map uniformly into several patches. Conversely, when large window attention sliding over the image, the current patch is allowed to query a larger area. For simplicity, we denote the query patch as $\mathbf{Q} \in \mathbb{R}^{P^2 \times C}$ and the queried large context patch as $\mathbf{C} \in \mathbb{R}^{R^2 \times P^2 \times C}$, where R is the ratio of the context patch size to the query patch size, and P^2 is the area of patch. Because the computational complexity of attention is

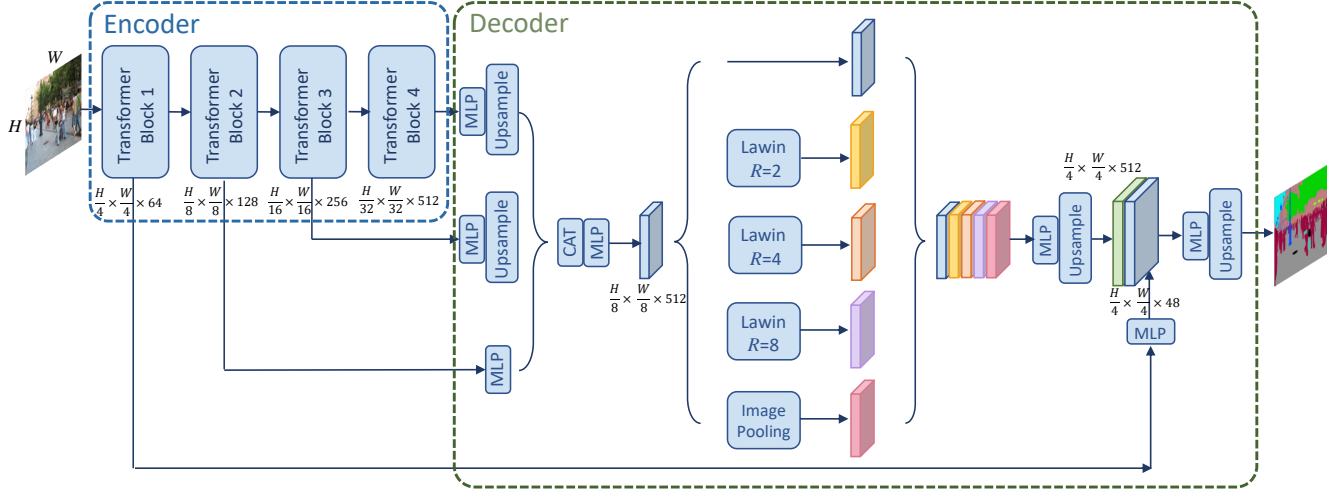


Figure 3. The overall structure of Lawin Transformer. The image is fed into the encoder part, which is a MiT. Then the features from the last three stages are aggregated and fed into the decoder part, which is a LawinASPP. Finally the resulted feature is enhanced with low-level information by the first-stage feature of encoder. "MLP" denotes the multi-layer perceptron. "CAT" denotes concatenating the features. "Lawin" denotes large window attention. "R" denotes the ratio of the size of context patch to query patch.

$O(P^2)$, when the spatial size of \mathbf{C} is increased by R times, the computational complexity increases to $O(R^2P^2)$. Under this circumstance, the computation of attention is not limited to the $P \times P$ local patch, and even unaffordable if ratio R or input resolution is very large. To preserve the original computational complexity, we pool \mathbf{C} to an abstract tensor with a downsampling ratio of R , reducing the spatial size of context patch back to (P, P) . However, there are certain drawbacks associated with such an easy process. The downsampling of context patch inevitably discards the abundant dependencies between \mathbf{Q} and \mathbf{C} especially as R is large. To mitigate the inattention, we naturally adopt the multi-head mechanism and let the number of head strictly equal to R^2 , thereby formulating the attention matrix from (P^2, P^2) to (R^2, P^2, P^2) . It is notable that the number of head has no impact on the computational complexity.

There has been researches revealing that, with certain techniques regularizing the head subspace, multi-head attention can learn desired diverse representations [12, 16, 18]. Considering that the spatial information becomes abstract after downsampling, we intend to strengthen the spatially representational power of multi-head attention. Motivated by that in MLP-Mixer the token-mixing MLP is complementary to channel-mixing MLP for gathering spatial knowledge, we define a set of head-specific *position-mixed* MLP = $\{\text{MLP}_1, \text{MLP}_2, \dots, \text{MLP}_h\}$. As illustrated in Fig. 2, every head of the pooled context patch is pushed into its corresponding token(position)-mixing MLP, and spatial positions within the same head communicate each other in an identical behavior. We term the resulting context as *position-mixed* context patch and denote it as \mathbf{C}^P , which is

calculated by:

$$\hat{\mathbf{C}} = \text{Reshape}(h, C/h, P^2)(\varphi(\mathbf{C})), \quad (8)$$

$$\mathbf{C}_h = \text{MLP}_h(\hat{\mathbf{C}}_h) + \hat{\mathbf{C}}_h, \quad (9)$$

$$\mathbf{C}^P = \text{Reshape}(C, P^2)(\text{concat}[\mathbf{C}_1; \mathbf{C}_2; \dots; \mathbf{C}_h]), \quad (10)$$

where $\hat{\mathbf{C}}_h$ denotes the h -th head of $\hat{\mathbf{C}}$ and $\text{MLP}_h \in \mathbb{R}^{P^2 \times P^2}$ is the h -th transformation strengthening the spatial representations for the h -th head, and φ denotes the average pooling operation. With the *position-mixed* context \mathbf{C}^P , we can reformulate the Eq. (3) and Eq. (4) as follows:

$$A = \text{softmax}\left(\frac{(\mathbf{W}_q \mathbf{Q}_h)(\mathbf{W}_k \mathbf{C}_h^P)^T}{\sqrt{D_h}}\right)(\mathbf{W}_v \mathbf{C}_h^P), \quad (11)$$

$$\text{MHA} = \text{concat}[A_1; A_2; \dots; A_h] \mathbf{W}_{\text{mha}}. \quad (12)$$

One primary concern is on the overhead of MLP, so we list the computational complexity of *local window attention* and *large window attention*:

$$\Omega(\text{Lowin}) = 4(HW)C^2 + 2(HW)P^2C, \quad (13)$$

$$\Omega(\text{Lawin}) = 4(HW)C^2 + 3(HW)P^2C, \quad (14)$$

where H and W are the height and width of entire image respectively, and P is the size of local window. Since P^2 , usually set to 7 or 8, is much smaller than C in high-level features, the extra expense induced by MLP is reasonably neglectable. It is admirable that the computational complexity of large window attention is independent of the ratio R .

3.3. LawinASPP

To capture multi-scale representations, we adopt the architecture of spatial pyramid pooling (SPP) to collaborate with large window attention and get the novel SPP module called LawinASPP. LawinASPP consists of 5 parallel branches including one shortcut connection, three large window attentions with $R = (2, 4, 8)$ and an image pooling branch. As shown in Fig. 3, branches of large window attention provide three hierarchies of receptive fields for the local window. Following the previous literature on window attention mechanism [30], we set the patch size of local window to 8, thus the provided receptive fields are of $(16, 32, 64)$. The image pooling branch uses a global pooling layer to obtain the globally contextual information and push it into a linear transformation followed by a bilinearly upsampling operation to match the feature dimension. The short path copies the input feature and paste it when all contextual information is output. All resulting features are first concatenated, and a learned linear transformation performs dimensionality reduction for generating the final segmentation map.

3.4. Lawin Transformer

Having investigated the advanced HVTs, we select the MiT and Swin-Transformer as the encoder of Lawin Transformer. MiT is designed for serving as encoder of SegFormer [43] which is a simple, efficient yet powerful semantic segmentation ViT. Swin-Transformer [30] is an extremely successful HVT built upon local window attention. Prior to applying LawinASPP, we concatenate the multi-level features with *output stride* = $(8, 16, 32)$ by resizing them to the size of feature with *output stride* = 8 and use a linear layer to transform the concatenation. The resulting transformed feature with *output stride* = 8 is fed into the LawinASPP and then we obtain the feature with multi-scale contextual information. In the state-of-the-art ViT for semantic segmentation, the feature for final prediction of segmentation logits is always derived from 4-level features of encoder. We hence employ the first-level feature with *output stride* = 4 to compensate low-level information. The output of LawinASPP is upsampled to the size of a quarter of input image, then fused with the first-level feature by a linear layer. Finally, the segmentation logits are predicted on the low-level-enhanced feature. More details are illustrated in Fig. 3

4. Experiments

Datasets: We conduct experiments on three public datasets including Cityscapes [17], ADE20K [53] and COCO-Stuff [4]. Cityscapes is an urban scene parsing dataset containing 5,000 fine-annotated images captured from 50 cities with 19 semantic classes. There are 2,975 images divided

into training set, 500 images divided into validation set and 1,525 images divided into testing set. ADE20K is one of the most challenging datasets in semantic segmentation. It consists of a training set of 20,210 images with 150 categories, a testing set of 3,352 images and a validation set of 2,000 images. COCO-Stuff is also a very challenging benchmark consists of 164k images with 172 semantic classes. The training set contains 118k images, and the test-dev dataset contains 20k images and the validation set contains of 5k images

Implementation Details: Our experiment protocols are exactly the same as those of [43]. Specially, we use the publicly available ImageNet1K-pretrained MiT [43] as the encoder of Lawin Transformer. All experiments in this section are implemented based on MMSegmentation [15] codebase on a server with 8 Tesla V100. When doing the ablation study, we choose MiT-B3 as encoder and train all models for 80k iterations. Unless specified, all results are achieved by single-scale inference. Note that all results of other methods are obtained by ours training the official code.

4.1. Comparison with SegFormer

To demonstrate the improved efficiency of Lawin Transformer, we compare it with SegFormer [43]. Both of them is built upon window attention and takes MiT as encoder. To enable fairness, we reimplement SegFormer in our environment. Table 1 shows the comparison on parameters, FLOPs and mIoU. Apparently, across all variants of MiT (B0→B5), Lawin Transformer trumps SegFormer on mIoU and FLOPs at a little extra parameters. When the light-weight MiT-B0 and MiT-B1 serve as encoder, Lawin Transformer can improve the performance with an adorable saving of computation cost. For example, Lawin-B0 uses much less FLOPs (by 3.1) to obtain a gain of 0.5% mIoU on COCO-Stuff dataset, and a gain of 0.8% on ADE20K dataset. Moreover, we observe that in some cases, Lawin Transformer can bridge the performance gap caused by the model capacity of encoder. For instance, SegFormer-B3 performs worse than SegFormer-B4 on all three datasets. But if replacing the original decoder with LawinASPP, the resulted Lawin-B3 outperforms SegFormer-B4 by 0.6% mIoU and yields a computation saving of 34G FLOPs on ADE20K, even using much less parameters. Also, on Cityscapes, Lawin-B4 improves over SegFormer-B5 by 0.4% with nearly a third less computation cost, Lawin-B3 improves over SegFormer-B5 by 0.2% with nearly a half less computation cost and parameters. These empirical results suggest that semantic segmentation ViT could encounter a performance bottleneck as the capacity of encoder continues to increase. In contrast with simply enlarging the encoder, LawinASPP presents a promising and efficient way to overcome the bottleneck by capturing the rich contextual information.

Dataset		ADE20K		Cityscapes		COCO-Stuff	
Method	Params(M) \downarrow	FLOPs(G) \downarrow	mIoU(SS/MS) \uparrow	FLOPs(G) \downarrow	mIoU(SS/MS) \uparrow	FLOPs(G) \downarrow	mIoU(SS) \uparrow
SegFormer-B0	3.8	8.4	38.1 / 38.6	125.5	76.5 / 78.2	8.4	35.7
Lawin-B0	4.1	5.3	38.9 / 39.6	99.3	77.2 / 78.7	5.3	36.2
SegFormer-B1	13.7	15.9	41.7 / 42.8	243.7	78.5 / 80.0	15.9	40.2
Lawin-B1	14.1	12.7	42.1 / 43.1	217.5	79.0 / 80.4	12.7	40.5
SegFormer-B2	27.5	62.4	46.5 / 47.5	717.1	81.0 / 82.2	62.4	44.5
Lawin-B2	29.7	45.0	47.8 / 48.8	562.8	81.7 / 82.7	45.0	45.2
SegFormer-B3	47.3	79.0	48.7 / 49.2	962.9	81.7 / 83.3	79.0	45.4
Lawin-B3	49.5	61.7	50.3 / 51.1	808.6	82.5 / 83.7	61.7	46.6
SegFormer-B4	64.1	95.7	49.6 / 50.4	1240.6	82.2 / 83.6	95.7	46.4
Lawin-B4	66.3	78.2	50.7 / 51.4	1086.2	82.7 / 83.8	78.2	47.3
SegFormer-B5	84.7	183.3	50.7 / 51.2	1460.4	82.3 / 83.7	111.6	46.7
Lawin-B5	86.9	159.1	52.3 / 53.0	1306.4	82.8 / 83.9	94.2	47.5

Table 1. Comparison of SegFormer with Lawin Transformer.

Method	FLOPs(G) \downarrow	Params(M) \downarrow	mIoU(SS/MS) \uparrow
Uper-T	236.1	59.9	44.5 / 45.8
Mask-T	59.0	41.8	46.7 / 48.8
Lawin-T	48.9	34.5	45.3 / 46.9
Uper-S	259.3	81.3	47.7 / 49.6
Mask-S	79.0	63.1	49.8 / 51.0
Lawin-S	72.0	55.9	48.7 / 50.4
Uper [†] -B [*]	470.4	121.4	51.6 / 53.0
Mask [†] -B [*]	195.0	101.9	52.7 / 53.9
Lawin [†] -B [*]	172.9	94.5	53.0 / 54.3
Uper [†] -L [*]	646.4	233.4	52.7 / 54.1
Mask [†] -L [*]	375.0	212.0	54.1 / 55.6
Lawin [†] -L [*]	350.6	201.2	54.7 / 56.2

Table 2. Comparison of Swin-Lawin Transformer with MaskFormer and Swin-UperNet on ADE20K. The method marked with \dagger takes cropped input of 640×640 . The method marked with $*$ indicates that its encoder is pretrained on ImageNet22k.

Method	FLOPs(G)	Params(M)	mIoU
PSP [50]	48.2	49.8	47.8
ASPP [9]	82.9	57.0	48.5
SEP-ASPP [10]	57.2	50.7	48.2
LawinASPP	61.7	49.5	49.9

Table 3. Results of different SPP modules when coupled with MiT-B3 on ADE20K.

4.2. Comparison with UperNet and MaskFormer

To further show the efficiency, we replace MiT with Swin-Transformer [30] and compare the Swin-Lawin Transformer with Swin-UperNet and MaskFormer on ADE20K as shown in table 2. From table 2, we have following observations. Firstly, compared with Swin-UperNet,

Swin-Lawin improves the performance largely and saves a great deal of computation cost. In particular, Lawin Transformer with Swin-B can outperform UperNet with Swin-L at nearly a quarter of its computation cost. Secondly, compared with Swin-MaskFormer, Swin-Lawin consistently uses less FLOPs and parameters across all variants of Swin-Transformer. Finally, through a closer look at performance, we find that Swin-Lawin performs worse than MaskFormer when the capacity of encoder is small (Swin-T \rightarrow S). However, as the capacity of encoder increases (Swin-B \rightarrow L), Swin-Lawin outperforms MaskFormer. It can be seen that with the increase of capacity, the performance gain created by Swin-Lawin compared with Swin-Uper also become larger. We infer that the short path branch and the low-level information in Lawin Transformer have very important roles in the final prediction (Sec 4.3.3 discusses the contribution of different hierarchies in Lawin Transformer), which both arise from the multi-level feature of backbone directly. So the more powerful the encoder part, the greater the performance gain from Lawin Transformer.

4.3. Ablation Study

4.3.1 Spatial Pyramid Pooling

Thanks to the spatial pyramid pooling (SPP) [23, 27] architecture in LawinASPP, Lawin Transformer captures multi-scale representations with large window attention in an efficient manner. To study the impact of large window attention and SPP architecture on performance, we choose some representative methods relying on SPP including PPM (Pyramid Pooling Module) [50], ASPP (Atrous Spatial Pyramid Pooling) [9] and SEP-ASPP (Depthwise Separable Atrous Spatial Pyramid Pooling) [10]. The sharp distinction between LawinASPP with these alternatives is the basic pool-

Ratio	Head	C-Mixing	P-Mixing	mIoU
(1,1,1)	(1,1,1)	✗	✗	48.6
(2,4,8)	(1,1,1)	✗	✗	47.3
(2,4,8)	(4,16,64)	✗	✗	47.9
(2,4,8)	(4,16,64)	✓	✗	49.1
(2,4,8)	(4,16,64)	✗	✓	49.9
(2,4,8)	(4,16,64)	✓	✓	49.4

Table 4. Results of Lawin-B3 with a variety settings of the ratio, head and MLP type on ADE20K.



Figure 4. A simple implementation of LawinASPP. The area of both query patch and context patch is set to (64,32,16)

Pooling Ratio	Head	Size	FLOPs(G)	mIoU
(1,2,4)	(1,4,16)	16	74.6	49.9
(2,4,8)	(4,16,64)	8	61.7	49.9
(4,8,16)	(16,64,256)	4	58.0	49.1

Table 5. Results of Lawin-B3 on ADE20k with context patch of different spatial sizes. "Size" means the spatial size of pooled context.

ing operator. PPM uses pyramid adaptive pooling to capture contextual information at different scales. ASPP uses the atrous convolution to extract multi-scale features. SEP-ASPP uses the depthwise separable atrous convolution [13] in the place of atrous convolution for the sake of efficiency. Table 3 shows parameters, FLOPs and mIoU when MiT-B3 combined with different SPP-based module, which are tested on ADE20K. PPM and SEP-ASPP are impressively computational economical, even using less FLOPs than LawinASPP. However there is a considerable performance gap between them and LawinASPP (2.1% for PPM, 1.7% for SEP-ASPP). ASPP achieves a slightly higher performance than SEP-ASPP, but spends the most computational resources. Through these competitions, LawinASPP proves to be the preferred module to introduce multi-scale representations into the semantic segmentation ViT, which is mainly attributed to *large window attention*.

4.3.2 Key Component in Large Window Attention

Pooling and Multi-Head: Pooling the large context patch with a downsampling ratio R and increasing the head number of MHA to R^2 purpose to reducing the computational complexity and recovering the discarded dependencies respectively. To verify the strategy, we implement the first

OS=4	Short Path	$R=2$	$R=4$	$R=8$	GAP	mIoU
✓	✓	✓	✓	✓	✓	49.9
✓	✓	✗	✓	✓	✓	49.5
✓	✓	✓	✗	✓	✓	49.4
✓	✓	✓	✓	✓	✗	49.4
✓	✗	✓	✓	✓	✓	48.9
✓	✓	✓	✓	✓	✗	49.3
✗	✓	✓	✓	✓	✓	49.1

Table 6. Results of Lawin-B3 on ADE20k when different branches are absent.

group experiments shown in table 4. We first test the performance when the large context patch keeps the spatial size without any downsampling. However, the required memory of this setting is unaffordable so we do a little tweak as illustrated in Fig. 4, setting the size of query patch equal to context patch. The performance of this simple implementation is lower than the standard implementation by 1.3%. If the context patch is pooled to the same size of query patch, the performance degrades severely, only achieving a 47.3% mIoU, owing to the sparsity of attention. Enabling multi-head mechanism can bring an improvement of 0.6%, but falling behind the standard and even the simple implementation. This group comparison shows that large window attention with the pooled context patch actually suffers inadequate dependencies, and the multi-head mechanism can alleviate it marginally.

Position-Mixing and Channel-Mixing: In large window attention, we innovatively employ the *position-mixing* operation to strengthen the spatially representational power of multi-head attention. In MLP-Mixer [37], the channel-mixing MLP is applied to learn knowledge of feature channels. That MLP-Mixer uses both kinds of MLPs prompts our investigation of *channel-mixing*. We enhance the communication along feature channels within each head by replacing the token-mixing MLP with channel-mixing MLP. The context patch is downsampled and the multi-head mechanism is enabled. The second group of results listed in table 4 shows that the channel-mixing MLP boosts the representation of multi-head attention and provides an appreciable performance improvement of 1.2%, but not powerful as token-mixing MLP (2%). Furthermore, we make a combination of token-mixing MLP with channel-mixing MLP, like a block in MLP-Mixer, to transform each head subspace along two dimensions, which attains a competitive result of 49.4% mIoU but worse than isolated *position-mixing* (49.9%). With these observations, we argue that the *position-mixing* operation is more useful than *channel-mixing* for recovering the dependencies of spatial downsampling operation.

Method	Backbone	FLOPs(G)↓	MS(%)↑
PSPNet [50]	ResNet101	2049	80.0
GCNet [5]	ResNet101	2203	80.7
PSANet [51]	ResNet101	2178	80.9
NonLocal [40]	ResNet101	2224	80.9
DeeplabV3 [9]	ResNet101	2781	80.8
CCNet [26]	ResNet101	2225	80.7
DANet [21]	ResNet101	2221	82.0
DNL [45]	ResNet101	2224	80.7
OCNet [49]	ResNet101	1820	81.6
DeeplabV3+ [10]	ResNet101	2032	82.2
SETR-PUP [52]	ViT-L*	—	82.2
Segmenter [36]	VIT-L*	—	81.3
SegFormer [43]	MiT-B5	1460	83.5
SegFormer [†]	MiT-B5	1460	83.7
Lawin	MiT-B5	1306	83.7
Lawin [†]	MiT-B5	1306	83.9
Lawin	Swin-L*	1797	84.2
Lawin [†]	Swin-L*	1797	84.4

Table 7. Performance Comparison on Cityscapes. The backbone marked with * indicates that it is pretrained on ImageNet22K. The method marked with † takes cropped input of 1024×1024 .

Spatial Size of Context: That large window attention pools the context patch to the same spatial size of query patch keeps the balance between efficiency and performance. We are interested in the consequence of disturbing the balance. To be specific, we evaluate the performance in following situations that the context patch is pooled to the spatial size of two times query patch and the context patch is pooled to the half size of query patch. The former sacrifices the computational economy and might be advantageous to performance, and the latter saves more computation cost and might be harmful to performance. It can be found in table 5 that no apparent performance is obtained in the former case. When the context patch is pooled to a smaller size, the mIoU drops 0.8% and only saves a little computation cost of 3.7G. Pooling the context patch to the size of query patch is a sensible choice keeping the balance well.

4.3.3 Branch in LawinASPP

As illustrated in Fig. 3, LawinASPP aggregates features derived from five branches to gather rich contextual information at multiple scales. Following the aggregation, the first-level feature comes to enhance it with low-level information via an auxiliary branch. We here study the efficacy of the six branches in LawinASPP. In table 6, we report the results when different branches are absent. For the branches of large window attention, the performance drops 0.4%, 0.5% and 0.5% for removing the branch with $R = 2$, $R = 4$ and

Method	Backbone	FLOPs(G)↓	MS(%)↑
PSPNet [50]	ResNet101	256	45.4
GCNet [5]	ResNet101	276	45.2
PSANet [51]	ResNet101	272	45.4
NonLocal [40]	ResNet101	278	45.8
DeeplabV3 [9]	ResNet101	348	46.7
CCNet [26]	ResNet101	278	45.0
DANet [21]	ResNet101	278	45.0
DNL [45]	ResNet101	278	45.8
OCNet [49]	ResNet101	227	45.4
DeeplabV3+ [10]	ResNet101	255	46.4
OCRNet [48]	HRNetW48	165	44.9
SETR-MLA [†] [52]	ViT-L*	—	50.3
Segmenter [†] [36]	ViT-L*	—	53.6
SegFormer [†] [43]	MiT-B5	183	51.2
Lawin [†]	MiT-B5	159	53.0
Swin-Upper [†] [30]	Swin-L*	646	54.1
MaskFormer [†] [11]	Swin-L*	375	55.6
Lawin [†]	Swin-L*	351	56.2

Table 8. Performance Comparison on ADE20K. The backbone marked with * indicates that it is pretrained on ImageNet22K. The method marked with † takes cropped input of 640×640 .

Method	Backbone	FLOPs(G)↓	mIoU(%)↑
NonLocal [40]	ResNet101	278	37.9
DeeplabV3+ [10]	ResNet101	255	38.4
OCRNet [48]	HRNetW48	165	42.3
SETR-MLA [52]	ViT-L*	—	45.8
SegFormer [43]	MiT-B5	112	46.7
Lawin	MiT-B5	94	47.5

Table 9. Performance Comparison on COCO-Stuff. The backbone with superscript * indicates that it is pretrained on ImageNet22K.

$R = 8$ respectively. The image pooling branch yields an improvement of 0.6% so the global contextual information is an essential hierarchy of LawinASPP. The short path is also indispensable to LawinASPP in that the biggest performance gain of (1.0%) is from this branch. We surprisingly observe that adding the auxiliary branch leads to an improvement of 0.8%, which manifests the importance of low-level information.

4.4. Comparison with State-of-the-Art

Finally, we compare our results with existing approaches on the ADE20K, Cityscapes and COCO-Stuff datasets.

Table 7 shows the results of state-of-the-art methods on Cityscapes dataset. The first group contains the CNN-based semantic segmentation method and the second group contains the ViT-based semantic segmentation method. If

not specified, the crop size of input image is $768/769 \times 768/769$. To boost the performance of Lawin Transformer, we use MiT-B5 and Swin-L as the encoder. Lawin Transformer with Swin-L achieves the best performance on Cityscapes.

Table 8 reports the performance of state-of-the-art methods on ADE20K dataset. The results are still grouped into two parts consists of CNN-based methods and ViT-based methods. If not specified, the crop size of input image is 512×512 . Lawin Transformer with Swin-L outperforms all other methods. Lawin Transformer with MiT-B5 uses the least FLOPs (159 GFLOPs) and achieves an excellent performance (53.0% mIoU).

Table 9 lists some results of state-of-the-art methods on COCO-stuff. Since there are few paper reporting the performance on COCO-Stuff, we just list the result of representative CNN-based methods. Lawin-B5 obtains the best mIoU of 47.5% and also uses the least FLOPs of 94G.

5. Conclusion

In this work, we develop an efficient semantic segmentation transformer called Lawin Transformer. The decoder part of Lawin Transformer is capable of capturing rich contextual information at multiple scales, which is established on our proposed *large window attention*. Compared to the existing efficient semantic segmentation Transformer, Lawin Transformer can achieve higher performance with less computational expense. Finally, we conduct experiments on Cityscapes, ADE20K and COCO-Stuff dataset, yielding state-of-the-art results on these benchmarks. We hope Lawin Transformer will inspire the creativity of semantic segmentation ViT in the future.

References

[1] Md Amirul Islam, Mrigank Rochan, Neil DB Bruce, and Yang Wang. Gated feedback refinement network for dense image labeling. In *Proceedings of the IEEE conference on computer vision and pattern recognition*, pages 3751–3759, 2017. 2

[2] Anurag Arnab, Mostafa Dehghani, Georg Heigold, Chen Sun, Mario Lučić, and Cordelia Schmid. Vivit: A video vision transformer. *arXiv preprint arXiv:2103.15691*, 2021. 2

[3] Vijay Badrinarayanan, Alex Kendall, and Roberto Cipolla. Segnet: A deep convolutional encoder-decoder architecture for image segmentation. *IEEE transactions on pattern analysis and machine intelligence*, 39(12):2481–2495, 2017. 2

[4] Holger Caesar, Jasper Uijlings, and Vittorio Ferrari. Coco-stuff: Thing and stuff classes in context. In *Proceedings of the IEEE conference on computer vision and pattern recognition*, pages 1209–1218, 2018. 2, 5

[5] Yue Cao, Jiarui Xu, Stephen Lin, Fangyun Wei, and Han Hu. Genet: Non-local networks meet squeeze-excitation networks and beyond. In *Proceedings of the IEEE/CVF International Conference on Computer Vision Workshops*, pages 0–0, 2019. 2, 8

[6] Nicolas Carion, Francisco Massa, Gabriel Synnaeve, Nicolas Usunier, Alexander Kirillov, and Sergey Zagoruyko. End-to-end object detection with transformers. In *European Conference on Computer Vision*, pages 213–229. Springer, 2020. 2

[7] Liang-Chieh Chen, George Papandreou, Iasonas Kokkinos, Kevin Murphy, and Alan L Yuille. Semantic image segmentation with deep convolutional nets and fully connected crfs. *arXiv preprint arXiv:1412.7062*, 2014. 2

[8] Liang-Chieh Chen, George Papandreou, Iasonas Kokkinos, Kevin Murphy, and Alan L Yuille. Deeplab: Semantic image segmentation with deep convolutional nets, atrous convolution, and fully connected crfs. *IEEE transactions on pattern analysis and machine intelligence*, 40(4):834–848, 2017. 2

[9] Liang-Chieh Chen, George Papandreou, Florian Schroff, and Hartwig Adam. Rethinking atrous convolution for semantic image segmentation. *arXiv preprint arXiv:1706.05587*, 2017. 1, 2, 6, 8

[10] Liang-Chieh Chen, Yukun Zhu, George Papandreou, Florian Schroff, and Hartwig Adam. Encoder-decoder with atrous separable convolution for semantic image segmentation. In *Proceedings of the European conference on computer vision (ECCV)*, pages 801–818, 2018. 1, 2, 6, 8

[11] Bowen Cheng, Alexander G. Schwing, and Alexander Kirillov. Per-pixel classification is not all you need for semantic segmentation. *arXiv*, 2021. 2, 8

[12] Rewon Child, Scott Gray, Alec Radford, and Ilya Sutskever. Generating long sequences with sparse transformers. *arXiv preprint arXiv:1904.10509*, 2019. 4

[13] François Chollet. Xception: Deep learning with depthwise separable convolutions. In *Proceedings of the IEEE conference on computer vision and pattern recognition*, pages 1251–1258, 2017. 7

[14] Xiangxiang Chu, Zhi Tian, Yuqing Wang, Bo Zhang, Haibing Ren, Xiaolin Wei, Huaxia Xia, and Chunhua Shen. Twins: Revisiting spatial attention design in vision transformers. *arXiv preprint arXiv:2104.13840*, 2021. 2

[15] MM Segmentation Contributors. MM Segmentation: Openmmlab semantic segmentation toolbox and benchmark. <https://github.com/open-mmlab/mmsegmentation>, 2020. 5

[16] Jean-Baptiste Cordonnier, Andreas Loukas, and Martin Jaggi. On the relationship between self-attention and convolutional layers. *arXiv preprint arXiv:1911.03584*, 2019. 4

[17] Marius Cordts, Mohamed Omran, Sebastian Ramos, Timo Rehfeld, Markus Enzweiler, Rodrigo Benenson, Uwe Franke, Stefan Roth, and Bernt Schiele. The cityscapes dataset for semantic urban scene understanding. In *Proceedings of the IEEE conference on computer vision and pattern recognition*, pages 3213–3223, 2016. 2, 5

[18] Stéphane d’Ascoli, Hugo Touvron, Matthew Leavitt, Ari Morcos, Giulio Biroli, and Levent Sagun. Convit: Improving vision transformers with soft convolutional inductive biases. *arXiv preprint arXiv:2103.10697*, 2021. 4

[19] Alexey Dosovitskiy, Lucas Beyer, Alexander Kolesnikov, Dirk Weissenborn, Xiaohua Zhai, Thomas Unterthiner, Mostafa Dehghani, Matthias Minderer, Georg Heigold, Sylvain Gelly, Jakob Uszkoreit, and Neil Houlsby. An image is worth 16x16 words: Transformers for image recognition at scale. In *ICLR*. OpenReview.net, 2021. [1](#) [2](#)

[20] Patrick Esser, Robin Rombach, and Bjorn Ommer. Taming transformers for high-resolution image synthesis. In *Proceedings of the IEEE/CVF Conference on Computer Vision and Pattern Recognition*, pages 12873–12883, 2021. [2](#)

[21] Jun Fu, Jing Liu, Haijie Tian, Yong Li, Yongjun Bao, Zhiwei Fang, and Hanqing Lu. Dual attention network for scene segmentation. In *Proceedings of the IEEE/CVF Conference on Computer Vision and Pattern Recognition*, pages 3146–3154, 2019. [2](#) [8](#)

[22] Ben Graham, Alaaeldin El-Nouby, Hugo Touvron, Pierre Stock, Armand Joulin, Hervé Jégou, and Matthijs Douze. Levit: a vision transformer in convnet’s clothing for faster inference. *arXiv preprint arXiv:2104.01136*, 2021. [2](#)

[23] Kristen Grauman and Trevor Darrell. The pyramid match kernel: Discriminative classification with sets of image features. In *Tenth IEEE International Conference on Computer Vision (ICCV’05) Volume 1*, volume 2, pages 1458–1465. IEEE, 2005. [1](#) [6](#)

[24] Junjun He, Zhongying Deng, and Yu Qiao. Dynamic multi-scale filters for semantic segmentation. In *Proceedings of the IEEE/CVF International Conference on Computer Vision*, pages 3562–3572, 2019. [1](#) [2](#)

[25] Junjun He, Zhongying Deng, Lei Zhou, Yali Wang, and Yu Qiao. Adaptive pyramid context network for semantic segmentation. In *Proceedings of the IEEE/CVF Conference on Computer Vision and Pattern Recognition*, pages 7519–7528, 2019. [1](#) [2](#)

[26] Zilong Huang, Xinggang Wang, Lichao Huang, Chang Huang, Yunchao Wei, and Wenyu Liu. Cenet: Criss-cross attention for semantic segmentation. In *Proceedings of the IEEE/CVF International Conference on Computer Vision*, pages 603–612, 2019. [2](#) [8](#)

[27] Svetlana Lazebnik, Cordelia Schmid, and Jean Ponce. Beyond bags of features: Spatial pyramid matching for recognizing natural scene categories. In *2006 IEEE Computer Society Conference on Computer Vision and Pattern Recognition (CVPR’06)*, volume 2, pages 2169–2178. IEEE, 2006. [1](#) [6](#)

[28] Hanchao Li, Pengfei Xiong, Jie An, and Lingxue Wang. Pyramid attention network for semantic segmentation. *arXiv preprint arXiv:1805.10180*, 2018. [2](#)

[29] Guosheng Lin, Anton Milan, Chunhua Shen, and Ian Reid. Refinenet: Multi-path refinement networks for high-resolution semantic segmentation. In *Proceedings of the IEEE conference on computer vision and pattern recognition*, pages 1925–1934, 2017. [2](#)

[30] Ze Liu, Yutong Lin, Yue Cao, Han Hu, Yixuan Wei, Zheng Zhang, Stephen Lin, and Baining Guo. Swin transformer: Hierarchical vision transformer using shifted windows. *arXiv preprint arXiv:2103.14030*, 2021. [1](#) [2](#) [5](#) [6](#) [8](#)

[31] Jonathan Long, Evan Shelhamer, and Trevor Darrell. Fully convolutional networks for semantic segmentation. In *Proceedings of the IEEE conference on computer vision and pattern recognition*, pages 3431–3440, 2015. [2](#)

[32] Volodymyr Mnih and Geoffrey E Hinton. Learning to detect roads in high-resolution aerial images. In *European Conference on Computer Vision*, pages 210–223. Springer, 2010. [1](#)

[33] Chao Peng, Xiangyu Zhang, Gang Yu, Guiming Luo, and Jian Sun. Large kernel matters—improve semantic segmentation by global convolutional network. In *Proceedings of the IEEE conference on computer vision and pattern recognition*, pages 4353–4361, 2017. [2](#)

[34] Olaf Ronneberger, Philipp Fischer, and Thomas Brox. U-net: Convolutional networks for biomedical image segmentation. In *International Conference on Medical image computing and computer-assisted intervention*, pages 234–241. Springer, 2015. [1](#) [2](#)

[35] Mennatullah Siam, Sara Elkerdawy, Martin Jagersand, and Senthil Yogamani. Deep semantic segmentation for automated driving: Taxonomy, roadmap and challenges. In *2017 IEEE 20th international conference on intelligent transportation systems (ITSC)*, pages 1–8. IEEE, 2017. [1](#)

[36] Robin Strudel, Ricardo Garcia, Ivan Laptev, and Cordelia Schmid. Segmenter: Transformer for semantic segmentation. *arXiv preprint arXiv:2105.05633*, 2021. [1](#) [2](#) [8](#)

[37] Ilya Tolstikhin, Neil Houlsby, Alexander Kolesnikov, Lucas Beyer, Xiaohua Zhai, Thomas Unterthiner, Jessica Yung, Andreas Steiner, Daniel Keysers, Jakob Uszkoreit, et al. Mlp-mixer: An all-mlp architecture for vision. *arXiv preprint arXiv:2105.01601*, 2021. [2](#) [7](#)

[38] Hugo Touvron, Matthieu Cord, Matthijs Douze, Francisco Massa, Alexandre Sablayrolles, and Hervé Jégou. Training data-efficient image transformers & distillation through attention. In *International Conference on Machine Learning*, pages 10347–10357. PMLR, 2021. [1](#) [2](#)

[39] Wenhui Wang, Enze Xie, Xiang Li, Deng-Ping Fan, Kaitao Song, Ding Liang, Tong Lu, Ping Luo, and Ling Shao. Pyramid vision transformer: A versatile backbone for dense prediction without convolutions. *arXiv preprint arXiv:2102.12122*, 2021. [2](#)

[40] Xiaolong Wang, Ross Girshick, Abhinav Gupta, and Kaiming He. Non-local neural networks. In *Proceedings of the IEEE conference on computer vision and pattern recognition*, pages 7794–7803, 2018. [2](#) [8](#)

[41] Haiping Wu, Bin Xiao, Noel Codella, Mengchen Liu, Xiyang Dai, Lu Yuan, and Lei Zhang. Cvt: Introducing convolutions to vision transformers. *arXiv preprint arXiv:2103.15808*, 2021. [2](#)

[42] Tete Xiao, Yingcheng Liu, Bolei Zhou, Yuning Jiang, and Jian Sun. Unified perceptual parsing for scene understanding. In *Proceedings of the European Conference on Computer Vision (ECCV)*, pages 418–434, 2018. [1](#) [2](#)

[43] Enze Xie, Wenhui Wang, Zhiding Yu, Anima Anandkumar, Jose M Alvarez, and Ping Luo. Segformer: Simple and efficient design for semantic segmentation with transformers. *arXiv preprint arXiv:2105.15203*, 2021. [2](#) [5](#) [8](#)

[44] Haotian Yan, Zhe Li, Weijian Li, Changhu Wang, Ming Wu, and Chuang Zhang. Contnet: Why not use convolution and transformer at the same time? *arXiv preprint arXiv:2104.13497*, 2021. 2

[45] Minghao Yin, Zhuliang Yao, Yue Cao, Xiu Li, Zheng Zhang, Stephen Lin, and Han Hu. Disentangled non-local neural networks. In *European Conference on Computer Vision*, pages 191–207. Springer, 2020. 2, 8

[46] Changqian Yu, Jingbo Wang, Changxin Gao, Gang Yu, Chunhua Shen, and Nong Sang. Context prior for scene segmentation. In *Proceedings of the IEEE/CVF Conference on Computer Vision and Pattern Recognition*, pages 12416–12425, 2020. 2

[47] Fisher Yu and Vladlen Koltun. Multi-scale context aggregation by dilated convolutions. *arXiv preprint arXiv:1511.07122*, 2015. 1, 2

[48] Yuhui Yuan, Xilin Chen, and Jingdong Wang. Object-contextual representations for semantic segmentation. In *Computer Vision–ECCV 2020: 16th European Conference, Glasgow, UK, August 23–28, 2020, Proceedings, Part VI 16*, pages 173–190. Springer, 2020. 8

[49] Yuhui Yuan, Lang Huang, Jianyuan Guo, Chao Zhang, Xilin Chen, and Jingdong Wang. Ocnet: Object context network for scene parsing. *arXiv preprint arXiv:1809.00916*, 2018. 1, 8

[50] Hengshuang Zhao, Jianping Shi, Xiaojuan Qi, Xiaogang Wang, and Jiaya Jia. Pyramid scene parsing network. In *Proceedings of the IEEE conference on computer vision and pattern recognition*, pages 2881–2890, 2017. 1, 2, 6, 8

[51] Hengshuang Zhao, Yi Zhang, Shu Liu, Jianping Shi, Chen Change Loy, Dahua Lin, and Jiaya Jia. Psanet: Point-wise spatial attention network for scene parsing. In *Proceedings of the European Conference on Computer Vision (ECCV)*, pages 267–283, 2018. 2, 8

[52] Sixiao Zheng, Jiachen Lu, Hengshuang Zhao, Xiatian Zhu, Zekun Luo, Yabiao Wang, Yanwei Fu, Jianfeng Feng, Tao Xiang, Philip HS Torr, et al. Rethinking semantic segmentation from a sequence-to-sequence perspective with transformers. In *Proceedings of the IEEE/CVF Conference on Computer Vision and Pattern Recognition*, pages 6881–6890, 2021. 1, 2, 8

[53] Bolei Zhou, Hang Zhao, Xavier Puig, Sanja Fidler, Adela Barriuso, and Antonio Torralba. Scene parsing through ade20k dataset. In *Proceedings of the IEEE conference on computer vision and pattern recognition*, pages 633–641, 2017. 2, 5